Korean J. Chem. Eng., **28**(9), 1844-1850 (2011)
DOI: 10.1007/s11814-011-0026-4

Optimization of physical parameters of solid oxide fuel cell electrode using electrochemical model

Dong Hyun Jo, Jeong Hwan Chun, Ki Tae Park, Ji Won Hwang, Jeong Yong Lee, Hyun Wook Jung, and Sung Hyun Kim†

Department of Chemical and Biological Engineering, Korea University, Seoul 136-713, Korea
(*Received 4 August 2010 • accepted 31 January 2011*)

Abstract−To enhance the performance of anode-supported solid oxide fuel cell (SOFC), an electrochemical model has been developed in this study. The Butler-Volmer equation, Ohm's law and dusty-gas model are incorporated to predict the activation, ohmic and concentration overpotentials, respectively. The optimal cell microstructure and operating parameters for the best current-voltage (J-V) characteristics have been sought from the information of the exchange current density and gas diffusion coefficients. As the cell temperature rises, the activation and ohmic overpotentials decrease, whereas the concentration overpotential increases due to the considerable reduction of gas density at the elevated temperature despite the increased diffusion coefficient. Also, increasing the hydrogen molar fraction and operating pressure can further augment the maximum cell output. Since there exists an optimum electrode pore size and porosity for maximum cell power density, the graded electrode has newly been designed to effectively reduce both the activation and concentration overpotentials. The results exhibit 70% improved cell performance than the case with a non-graded electrode. This electrochemical model will be useful to simply understand overpotential features and devise the strategy for optimal cell design in SOFC systems.

Key words: SOFC, Simulation, Ohmic, Activation, Concentration, Overpotential, Graded Electrode, Performance of Fuel Cell

INTRODUCTION

The solid oxide fuel cell (SOFC) has been considered as a promising fuel cell for the direct conversion of chemical energy with its superior capability in co-generation systems by using the high temperature waste heat. Recently, the issues on the improvement of cell performance as the magnitude of power density generated by fuel cells at intermediated temperature have been extensively emphasized in SOFC systems.

According to the second law of thermodynamics, there exist losses of potentials in fuel cell performance owing to (1) ionic resistance through the electrolyte and electronic resistance in the electrodes and interconnects, (2) delay of reactions occurring on the electrode/electrolyte interface, and (3) the insufficient diffusion of gases to the reaction sites. The irreversibility of losses can be clarified numerically or experimentally. However, numerical models have been preferably adopted, considering their economical benefits and also difficulties with experimental works under high temperature operation. For instance, the role of electrode geometry and operating conditions on the electrochemical performance has been theoretically explored. Tanner et al. [1] revealed the improvement of cell performance by controlling the porous electrode structure. Bejan et al. [2] and Vargas et al. [3] completed a constructional theory on the optimization of single SOFC internal structure for obtaining maximum electrical power density. Hernandez-Rachesco et al. [4] elucidated the effect of hydrogen, methane and carbon monoxide as pure fuels on the performance by comparing the several models.

In this study, we evaluated the effects of operation conditions and electrode structure on the performance of SOFC by using modified Butler-Volmer equation, including temperature dependence of activation loss. In addition, we adopted graded electrode structure for anode which has gradients of porosity and pore size. We focused on electrochemical equations for investigating the key role of electrochemical nature in the cell performance. In addition, dusty-gas model and Ohm's law relation have been implemented in electrochemical models to determine the concentration and ohmic overpotentials, respectively.

ELECTROCHEMICAL MODELS

There are, in general, several numerical models employed to exploit the polarization terms in SOFCs [5]: micro-level [6-10], macro-level [11-14], and semi-empirical models [15-17]. Results shown in this paper are based on a macro-level model under the assumption that the reactions take place at the electrode/electrolyte interface, not requiring microscopic analysis. Although this assumption is not suitable for cermet-type anodes with electrode and electrolyte randomly intermixed, this will be one of useful models for anode-supported cells with thick anodes in that most of the polarization contribution occurs at the interface.

The external voltage (V) comprises an equilibrium voltage and various overpotentials in an SOFC.

$$V=E-\eta_{elec}-\eta_{ohmic}=E-\eta_{act,a}-\eta_{act,c}-\eta_{conc,a}-\eta_{conc,c}-\eta_{ohmic} \quad (1)$$

where E and η_{elec} are the equilibrium voltage (open circuit voltage)

†To whom correspondence should be addressed.
E-mail: kimsh@korea.ac.kr

and electrode overpotential. η_{elec} includes activation overpotential of the anode ($\eta_{act,a}$), activation overpotential of the cathode ($\eta_{act,c}$), concentration overpotential (η_{conc}) and ohmic overpotential of electrolyte (η_{ohmic}), respectively.

The equilibrium voltage, E, can be expressed by the Nernst equation.

$$E = E_0 + \frac{RT}{2F}\ln\left(\frac{P_{H_2}P_{O_2}^{1/2}}{P_{H_2O}}\right) \quad (2)$$

where R denotes the universal gas constant (8.3145 J/mol·K), F the Faraday constant (96,485 C/mol), T the absolute temperature, and P_{H_2}, P_{H_2O} and P_{O_2} the partial pressures of hydrogen, steam and oxygen, respectively.

1. Activation Overpotential

The external voltage is inevitably decreased by the slow reactions on the electrode/electrolyte interface. In other words, a portion of the voltage generated is lost for electron transfer to or from electrode during chemical reactions. The electrode activation overpotential-current density relationship can be represented by Butler-Volmer equation.

$$J = J_0\left[\exp\left(\frac{\alpha zF\eta_{act}}{RT}\right) - \exp\left(-\frac{(1-\alpha)zF\eta_{act}}{RT}\right)\right] \quad (3)$$

where J_0 is exchange current density which is the current at the reversible potential, z the number of electrons involved in reaction, and α the symmetrical factor. For a SOFC, z and α are set to 2 and 0.5, respectively. The activation overpotentials at anode ($\eta_{act,a}$) and cathode ($\eta_{act,c}$) can be written as

$$\eta_{act,i} = \frac{RT}{F}\sinh^{-1}\left(\frac{J}{2J_{0,i}}\right) = \frac{RT}{F}\ln\left[\frac{J}{2J_{0,i}} + \sqrt{\left(\frac{J}{2J_{0,i}}\right)^2 + 1}\right], \quad i = a, c \quad (4)$$

where indices a and c denote anode and cathode. $J_{0,i}$, playing a key role in altering activation overpotential, is strongly dependent on the electrode microstructure properties (e.g., porosity, pore size, and length of triple phase boundary (TPB)) and operating conditions (e.g., gas composition, operating temperature and pressure). It has recently been reported [18] that the length of the TPB can be determined by the grain size, porosity and pore diameter. Therefore, the exchange current density can be expressed in terms of the length of the TPB.

$$J_{0,i} \propto \frac{72X[D_P - (D_P + D_S)n]n}{D_S^2 D_P^2 (1 - X^2)} \quad (5)$$

where X represents the portion of contacting grain area, n the porosity, D_P the pore size, and D_S the grain size. All those parameters are set equal to both anode and cathode. Combining both the operating and microstructural parameters, the final form of the exchange current density can be given at anode and cathode electrodes.

$$J_{0,a} = k_a \frac{72X[D_P - (D_P + D_S)n]n}{D_S^2 D_P^2 (1 - X^2)} \times \left(\frac{P_{H_2}}{P_{ref}}\right)\left(\frac{P_{H_2O}}{P_{ref}}\right)\exp\left(-\frac{E_{act,a}}{RT}\right) \quad (6)$$

$$J_{0,c} = k_c \frac{72X[D_P - (D_P + D_S)n]n}{D_S^2 D_P^2 (1 - \alpha^2)} \times \left(\frac{P_{O_2}}{P_{ref}}\right)^{0.25}\exp\left(-\frac{E_{act,c}}{RT}\right) \quad (7)$$

where k_a, k_c are coefficients for the exchange current density at the anode and cathode, and $E_{act,a}$, $E_{act,c}$ are the activation energies at the anode and cathode, respectively.

2. Concentration Overpotential

The change of reactant concentrations at the electrode/electrolyte interface should be accounted for in potential loss because the reduction of concentrations readily leads to the insufficient reaction on the electrode/electrolyte interface. This type of loss is often called mass transport loss. For an SOFC, the concentration loss can be typically presented in terms of gas concentration difference between the electrode surface and electrode/electrolyte interface. The concentration overpotential of anode is shown as below.

$$\eta_{conc,a} = -\frac{RT}{2F}\ln\left(\frac{y_{H_2}y_{H_2O}^I}{y_{H_2O}y_{H_2}^I}\right) \quad (8)$$

where y_i represents molar fraction of species i and the superscript I indicates inlet conditions. The concentration overpotential of cathode could be neglected because the diffusion transport contribution is insignificant due to thin cathode (50 μm). The partial pressures at the electrolyte-electrode interface can be determined using dusty-gas model (DGM, Eq. (9)), considering both molecular and Knudsen diffusions of the gas in the porous electrode. The rate of mass transport according to the DGM is given by

$$\frac{N_i}{D_k^{eff}} + \sum_{j=1, j\neq i}^{n}\frac{y_jN_i - y_iN_j}{D_{i,j}^{eff}} = -\frac{P}{RT}\frac{dy_i}{dz} \quad (9)$$

where D_k^{eff}, $D_{i,j}^{eff}$ means effective Knudsen diffusion and molecular diffusion coefficients and N_i represents the rate of mass transport. This assumes that the pore walls consist of giant, motionless, pseudo molecules (dust) uniformly distributed in space. The molar flux is determined from the Graham's law of diffusion in gaseous mixtures. It is well known that the DGM is more accurate under dominant Knudsen diffusion condition where the pore size is much smaller than the mean free path of the molecular species [19]. To take into account the tortuosity (ξ) and porosity (ε) within electrodes, the effective molecular and Knudsen diffusivities in Eq. (9) are shown as follows [20,21].

$$D_{H_2-H_2O}^{eff} = \frac{\varepsilon}{\xi}D_{H_2-H_2O}, \quad D_{H_2,k}^{eff} = \frac{\varepsilon}{\xi}D_{H_2,k} \quad (10)$$

Using the above DGM, the relationship between compositions for the system, H_2-H_2O, at the electrode/electrolyte interfaces is set in Eqs. (11) and (12)

$$y_{H_2} + y_{H_2O} = 1 \quad (11)$$

$$\frac{d^2y_{H_2}}{dz^2} + \frac{\alpha}{D_{H_2-H_2O}^{eff}}\left\{\frac{1-\alpha y_{H_2}}{D_{H_2-H_2O}^{eff}} + \frac{1}{D_{H_2,k}^{eff}}\right\}\times\left(\frac{dy_{H_2}}{dz}\right)^2 = 0 \quad (12)$$

with the following boundary conditions:

$$y_{H_2}(0) = y_{H_2}^I \quad (13)$$

$$\left.\frac{dy_{H_2}}{dx}\right|_{x=0} = -j\frac{RT}{2pF}\left\{\frac{1-\alpha y_{H_2}^I}{D_{H_2-H_2O,e}} + \frac{1}{D_{H_2,k,e}}\right\} \quad (14)$$

where $\alpha = 1 - \sqrt{M_{H_2}/M_{H_2O}}$.

DGM equations have been solved by 4th-order Runge-Kutta method.

3. Ohmic Overpotentials

The loss due to the electrical resistance of the electrode and the

resistance to the flow of ions through the electrolyte is named the ohmic overpotential. The overall ohmic overpotential is primarily induced by relatively low ionic conductivity of electrolyte rather than by electric conductivity of electrodes. According to Ohm's law, the ohmic overpotential of the SOFC can be formulated in terms of properties of the electrolyte [22].

$$\eta_{ohmic} = 2.99\times10^{-5} JL\exp\left(\frac{10300}{T}\right) \quad (15)$$

where L represents the thickness of the electrolyte in units of meters.

RESULTS ON PARAMETRIC ANALYSIS

Many parameter values for this analysis have been chosen from the literature [20,23]. At first, values of the exchange current density (J_0) at anode and cathode are differently set to 5,300 and 2,000 A/m^2 at 1,073 K, respectively, as suggested in the literature [18,24]. Considering the temperature dependency of the exchange current density, their values at 1,023 K were modified as 3,800 and 1,285 A/m^2, respectively, by using Eqs. (6) and (7). As the typical operating pressures, P_{H_2O}, P_{H_2}, and P_{O_2} were selected to 0.03, 0.97 and 0.21 bar, respectively. The pore size and grain size were 2.4 μm and 1.5 μm. Values of all input parameters used in the present analysis are summarized in Table 1.

The micro-structure and the geometry of the electrode affect the relevant transport and reaction characteristics. The models in this study were employed to in-depth figure out features of the activation, ohmic, and concentration overpotentials of an SOFC under different operating conditions and then optimally establish cell performance.

Table 1. Input parameters used in SOFC electrochemical modeling [14]

Parameter	Value
Activation energy of anode $E_{act,a}$ (J/mol)	1.0×10^5
Activation energy of cathode $E_{act,a}$ (J/mol)	1.2×10^5
Operating temperature, T (K)	1023
Operating pressure, P (bar)	1.0
Hydrogen molar fraction at inlet, $y^I_{H_2}$	0.97
Anode porosity, n	0.42
Anode tortuosity, ξ	5.4
Average length of grain contact, X	0.7
Average pore radius, D_P	2.4
Average grain size, D_S	1.5
Typical anode-supported SOFC	
Anode thickness (μm)	1000
Electrolyte thickness (μm)	10
Cathode thickness (μm)	50

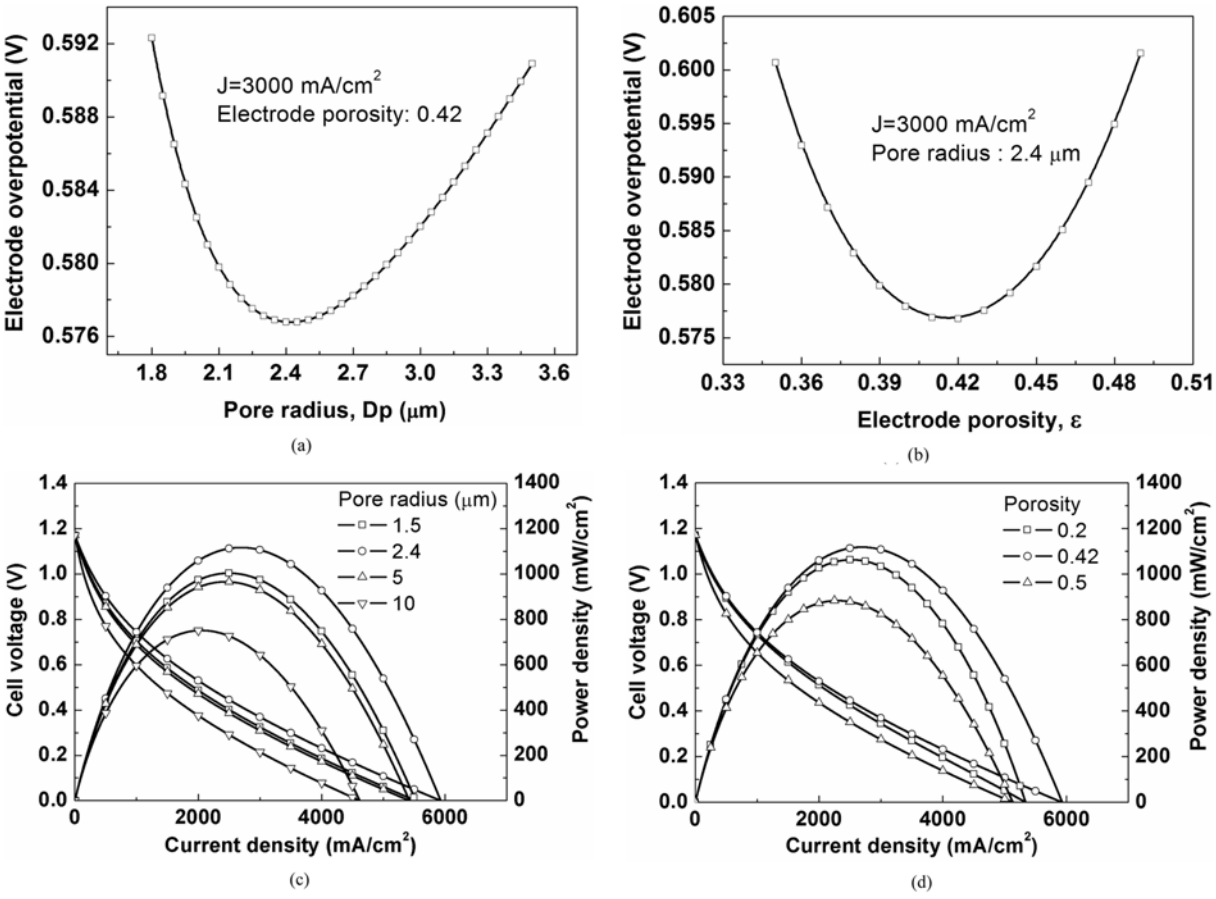

Fig. 1. Effect of electrode structure: (a) electrode overpotential with various pore radius, (b) electrode overpotential with various porosity, (c) cell performance with various pore radius and (d) cell performance with various porosity.

1. Effect of Cell Structure

1-1. Pore Size and Porosity

The TPB length, which is closely related with the pore size, grain size, and overlap of particles, principally affects the activation overpotential. Therefore, activation overpotential can be minimized at maximum TPB length by controlling the pore size and porosity. It is noted that the concentration overpotential decreases with increasing pore size and porosity due to the increased Knudsen diffusion. To see overall effects, optimal pore size and porosity are found to 2.4 μm (Fig. 1(a)) and 0.42 (Fig. 1(b)), respectively, clearly achieving the better cell performance in terms of cell voltage and power density (Figs. 1(c) and 1(d)).

1-2. Graded Electrode

As mentioned in the previous section for the porous electrode, there exist optimum pore size and porosity due to the length of the TPB and diffusion process in porous electrode. In typical non-graded electrode case, decreasing pore size and porosity for reducing activation overpotential makes the concentration overpotential greatly larger. Such opposing effect can be eliminated by a well-defined graded electrode. To effectively reduce both the activation and concentration overpotentials, a graded electrode was proposed [25]. It is similar to anode functional layer which was fabricated to optimize the microstructures of the anode [26]. Compared with non-graded electrode (Fig. 2(a)), a micro-structural graded electrode can be classified into two different types, namely porosity grading and pore size grading, respectively (Figs. 2(b) and 2(c)). It is assumed that both porosity and pore size increase from the electrode/electrolyte interface to the electrode surface, linearly.

The graded electrode can offer both sufficient reactive area and good gas transport. Employing the graded electrode model, optimal pore size and porosity at electrode/electrolyte interface has been predicted from activation overpotential to have the largest length of TPB, as shown in Fig. 3. The optimum pore size and porosity in this case are 2 μm and 0.3, respectively. If pore size and porosity are larger 5 μm and 0.6, respectively, the electrode will suffer from poor particle connectivity, poor percolation, and poor mechanical strength. Therefore, a linear grading in pore size in range from 2 μm to 5 μm is studied. In addition, a linear grading of porosity in the range from 0.3 to 0.6 is also analyzed. In Fig. 4 depicting the comparison of the cell performances in non-graded and graded electrodes, both pore size and porosity graded electrodes show almost same elevated cell performance, unlike the previous results [25].

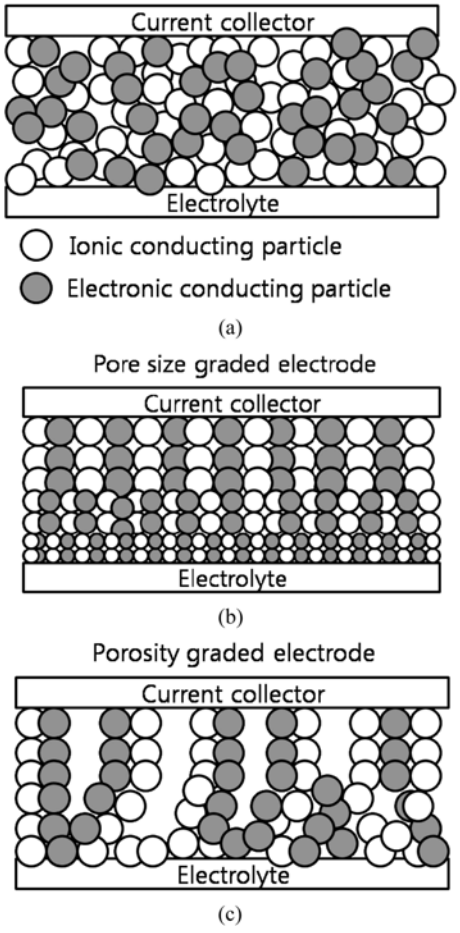

Fig. 2. Schematic diagram of (a) non-grading electrode consisting of both electronic conducting particles and ionic conducting particles, (b) functionally pore size graded anode and (c) porosity graded anode.

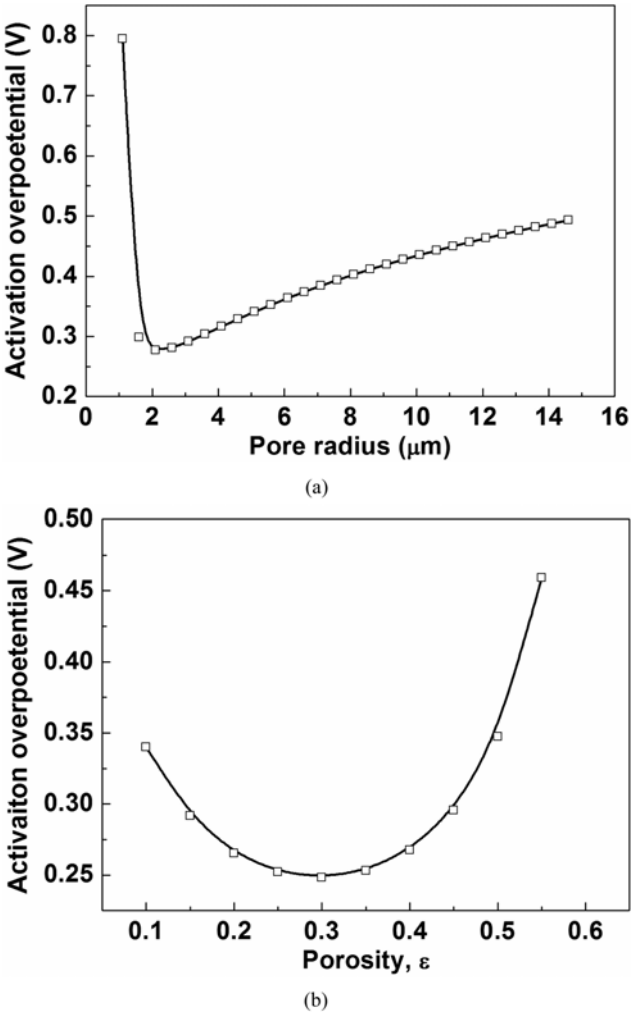

Fig. 3. Effect of electrode structure at electrode/electrolyte interface: (a) activation overpotential with varying pore size and (b) activation overpotential with varying porosity.

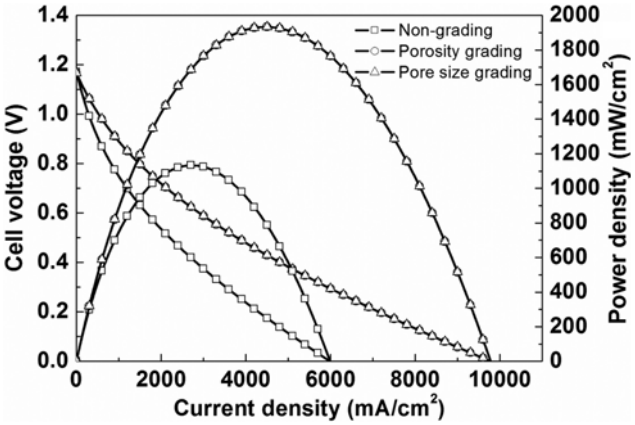

Fig. 4. Cell performance with non-graded anode and functionally graded anode.

This difference might be ascribed to the assumption that every reaction takes place in electrode/electrolyte interface. If the gross reaction inside the electrode is considered, the pore size graded electrode will give better performance than porosity graded one in that the former can provide much more reaction sites than the latter. The activation and concentration overpotentials are significantly reduced with the graded electrode, resulting in about 70% increase of the maximum power density in comparison to the non-graded electrode case.

2. Effect of Operating Conditions

The effect of conditions such as operating temperature, gas composition, and operating pressure on the cell performance have been analyzed in this section, using the optimized data for non-graded electrode achieved from section 1.

2-1. Operating Temperature

Operating temperature can affect the ohmic overpotential because the ion conductivity of the electrolyte varies with operating temperature. It is observed that the ohmic overpotential is significantly decreased with increasing operating temperature owing to the elevated ion conductivity of electrolyte. Nevertheless, the ohmic overpotential is still one of key factors to control cell performance at intermediate temperature range (923-1,023 K).

It is noted that the activation overpotential is also reduced with increasing operating temperature, resulting from more active electrodes and faster reaction rate at higher temperature. It was reported [8], however, the Butler-Volmer equation with constant exchange current density yielded increased activation overpotential with increasing operating temperature. This is because using constant exchange current density makes it impossible to reflect temperature dependency of reaction. Recently, the Butler-Volmer equation has been suggested considering temperature-dependency of the exchange current density, and it provides more realistic results and guarantees the good agreement with experimental findings [18,27]. We also used temperature-dependent exchange current density (Eqs. (6) and (7)) for the Butler-Volmer equation and acquire well-calculated activation overpotential with Eq. (4). (Fig. 5(a)).

In contrast to expectations, the concentration overpotential was found to rise with increasing operating temperature (Eq. (8)), as depicted in Fig. 5(b). This is because the gas density decreases with increasing temperature although the diffusion rate is raised with the

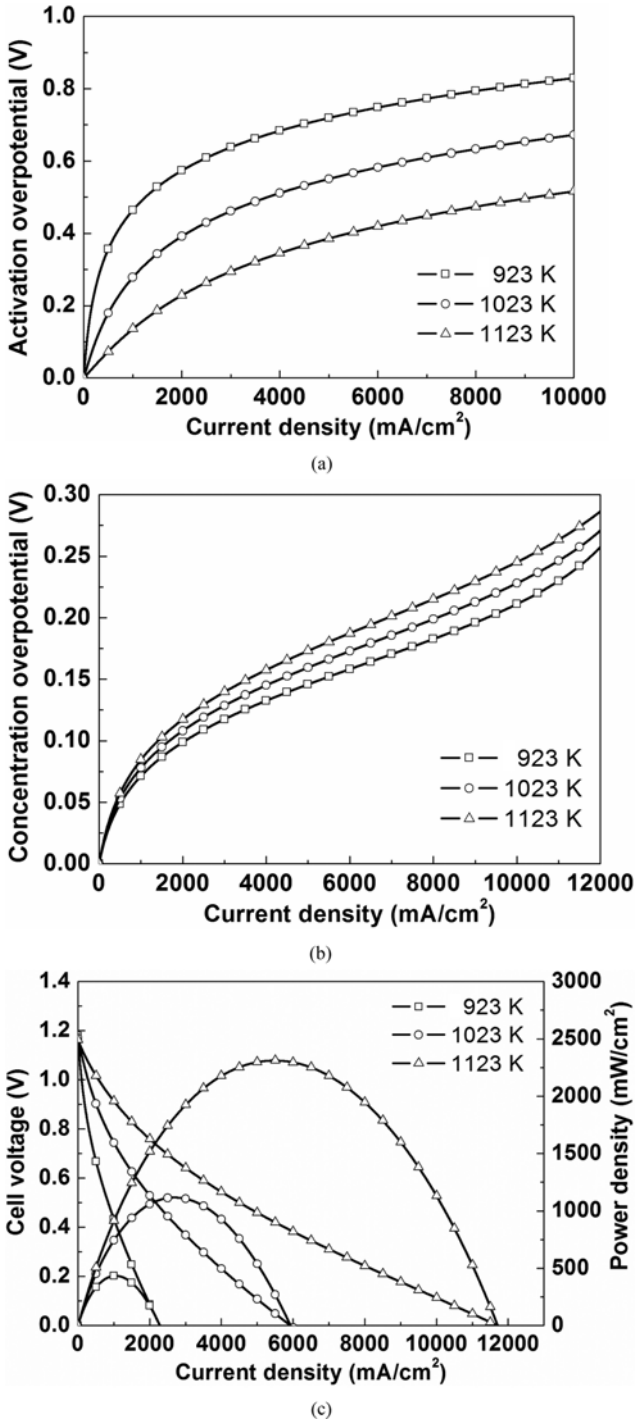

Fig. 5. Effect of operating temperature: (a) activation overpotential, (b) concentration overpotential and (c) J-V characteristics and power density.

temperature [28-31].

Consequently, the combined effects according to the variation of overpotentials resulted in better cell performance at higher temperature by reducing the activation and ohmic overpotentials, drastically (Fig. 5(c)).

2-2. Gas Composition

The activation overpotential was decreased with increasing concentration of hydrogen due to insufficient reactant. According to

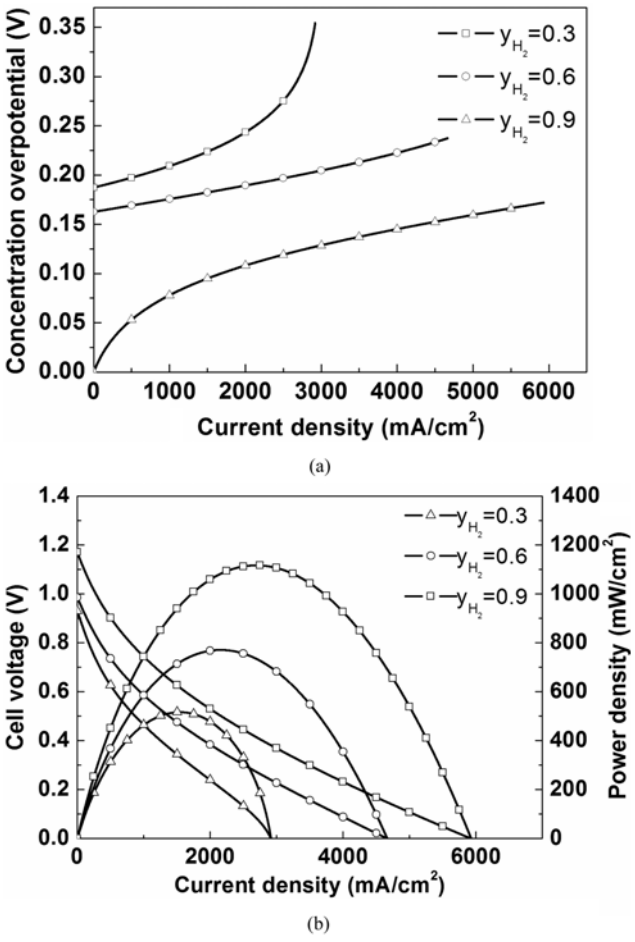

Fig. 6. Effect of hydrogen molar fraction: (a) concentration overpotential and (b) J-V characteristics and power density.

Eq. (6), the exchange current density of anode is decreased with decreasing of concentration of hydrogen. It reflects that there exists a lack of reaction at electrode/electrolyte interface due to the insufficient reactants. It was known that the concentration overpotential was more sensitive to the variation of $y^{l}_{H_2}$ than the activation overpotential [32]. Although it is considerably difficult to estimate the concentration overpotential in low $y^{l}_{H_2}$ condition at low current density region with the dusty-gas model, the concentration overpotential was greatly increased with decreasing $y^{l}_{H_2}$, as shown in Fig. 6(a). The resulting J-V characteristics and power density are demonstrated in Fig. 6(b).

2-3. Operating Pressure

Both activation and concentration overpotentials are decreased with increasing operating pressure. It is revealed that the diffusion procedure is less sensitive to the pressure. [27]. However, the gas density rises with increasing P, giving lower concentration overpotential. Also, the activation overpotential is reduced at a higher pressure because the porous electrode becomes more reactive with higher molar concentration. Furthermore due to the increase of partial pressures at a higher pressure, a little higher open circuit voltage can be acquired. As operating pressure increases, both activation and concentration overpotentials are decreased so that better cell performance is obtained, as shown in Fig. 7.

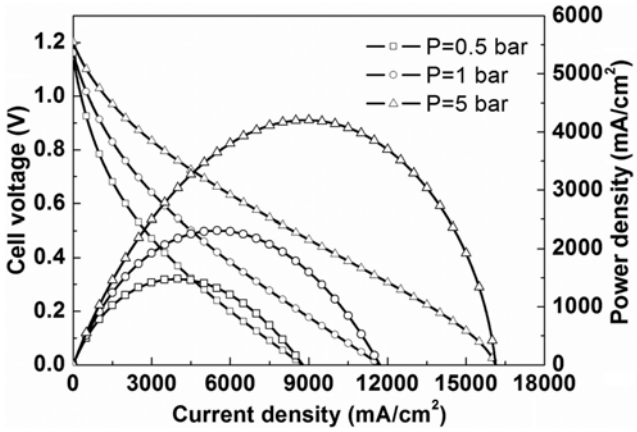

Fig. 7. Cell performance with various operating pressure.

CONCLUSION

The optimal electrode structure and operating conditions to improve the cell performance of anode-supported SOFC have been investigated using electrochemical models. Various models for describing the specified overpotentials have been involved in electrochemical equations. In addition, we introduced the graded electrode structure to decrease the cell overpotentials and conducted a comparison study with non-graded electrode structure. The optimal pore size and porosity have been readily sought, considering the overall effect of overpotentials in both non-graded and graded electrodes. For typical operating conditions, 1,023 K, 1 bar and hydrogen molar fraction of 0.97, optimum electrode pore radius of 2.4 μm and optimum porosity of 0.42 are found in the non-graded electrode. In addition, it has been revealed that linearly graded electrode gives 70% enhanced cell performance in comparison to the non-graded one. This is because the graded electrode can offer both sufficient reactive area and good gas transport so that both activation and concentration overpotential decrease simultaneously. In this case, optimum pore size and porosity of 2.2 μm and 0.3 are found to minimize activation overpotential at electrode/electrolyte interface. Accordingly, the determination of operating conditions and electrode structures is important to make an electrode which has minimized electrode overpotential. The electrochemical models applied in this study could help to design optimized electrode in SOFC.

ACKNOWLEDGEMENTS

This study was supported by research grants from Korea Energy Management Cooperation (KEMCO) and Korea Institute of Energy Technology Evaluation and Planning (KETEP).

NOMENCLATURE

d_a : anode thickness [μm]
$D_{H_2,k}$: knudsen diffusion coefficient of H_2 [m^2/s]
$D_{H_2-H_2O}$: molecular diffusion coefficient of H_2 and H_2O [m^2/s]
D_i^{eff} : effective diffusion coefficient of species i [m^2/s]
D_P : pore diameter [μm]
E : equilibrium potential [V]

$E_{act,a}$: activation energy at cathode [J/mol]
$E_{act,c}$: activation energy at cathode [J/mol]
F : faraday constant [9.6485×10^4 C/mol]
J : current density [mA/cm^2]
$J_{0,i}$: exchange current density (i=anode, cathode) [mA/cm^2]
k_i : coefficient for exchange current density (i=anode, cathode)
L : thickness of electrolyte [μm]
n : anode porosity
P : operating pressure [bar]
P_i : partial pressure of species i (i=H_2O, H_2, O_2 and reference) [bar]
R : universal gas constant [8.3145 J/mol·K]
T : operating temperature [K]
V : cell potential [V]
X : ratio of length of grain contact neck to grain size
y_i^I : molar fraction of species i in bulk [i=H_2O, H_2]
z : number of electrons evolved per reaction
$\eta_{act,a}$: activation overpotential at anode [V]
$\eta_{act,c}$: activation overpotential at cathode [V]
η_{conc} : concentration overpotential [V]
η_{ohmic} : ohmic overpotential [V]
ξ : anode tortuosity

Subscripts
a : anode
c : cathode

REFERENCES

1. C. W. Tanner, K. Z. Fung and A. V. Virkar, *J. Electrochem. Soc.*, **144**, 1 (1997).
2. A. Bejan, Cambridge University Press (2000).
3. J. C. Ordonez, S. Chen, J. V. C. Vargas, F. G. Dias, J. E. F. C. Gardolinski and D. Vlassov, *Int. J. Energy Res.*, **31**, 1337 (2007).
4. E. Hernandez-Racheco, D. Singh, P. N. Hutton, N. Patel and M. D. Mann. *J. Power Sources*, **138**, 174 (2004).
5. S. Kakac, A. Pramuanjaroenkij and X. Y. Zhou, *Int. J. Hydrog. Energy*, **32**, 761 (2007).
6. P. Costamagna, P. Costa and V. Antonucci, *Electrochem. Acta*, **43**(3-4), 375 (1998).
7. J. W. Kim, A. V. Virkar, K. Z. Fung, K. Mehta and S. C. Singhal, *J. Electrochem. Soc.*, **146**(1), 69 (1999).
8. S. Sunde, *J. Electroceram.*, **5**(2), 153 (2000).
9. J. Divisek, R. Jung and I. C. Vinke, *J. Appl. Electrochem.*, **29**, 165 (1999).
10. S. H. Chan and Z. T. Xia, *J. Electrochem. Soc.*, **148**(4), A388 (2001).
11. S. H. Chan, K. A. Khor and Z. T. Xia, *J. Power Sources*, **93**, 130 (2001).
12. H. Zhu and R. J. Kee, *J. Power Sources*, **117**, 61 (2003).
13. W. Lehnert, J. Meusinger and F. Thom, *J. Power Sources*, **87**, 57 (2000).
14. H. Yakabe, M. Hishinuma, M. Uratani, Y. Matsuzaki and I. Yasuda, *J. Power Sources*, **86**, 423 (2000).
15. E. Achenbach, *J. Power Sources*, **49**, 333 (1994).
16. H. Yakabe, T. Ogiwara, M. Hishinuma and I. Yasuda, *J. Power Sources*, **102**, 144 (2001).
17. M. Iwata, T. Hikosaka, M. Morita, T. Iwanari, K. Ito, K. Onda, Y. Esaki, Y. Sakaki and S. Nagata, *Solid State Ionics*, **132**, 297 (2000).
18. X. H. Deng and A. Petric, *J. Power Sources*, **140**(2), 297 (2005).
19. R. Suwanwarangkul, E. Croiset, M. W. Fowler, P. L. Douglas, E. Entchev and M. A. Douglas, *J. Power Sources*, **122**, 9 (2003).
20. S. H. Chan, K. A. Khor and Z. T. Xia, *J. Power Sources*, **93** 130 (2001).
21. H. Zhu and R. J. Kee, *J. Power Sources*, **117**, 61 (2003).
22. J. R. Ferguson, J. M. Fiard and R. Herbin, *J. Power Sources*, **58**(2), 109 (1996).
23. A. Ringuede, D. Bronine and J. R. Frade, *Solid State Ionics*, **146**(3-4), 219 (2002).
24. S. H. Chan and Z. T. Xia, *J. Appl. Electrochem.*, **32**(3), 339 (2002).
25. M. Ni, M. K. H. Leung and D. Y. C. Leung, *J. Power Sources*, **168**, 369 (2007).
26. J. Kong, K. Sun, D. Zhou, N. Zhang, J. Mu and J. Qiao, *J. Power Sources*, **166**, 337 (2007).
27. M. Ni, M. K. H. Leung and D. Y. C. Leung, *Energy Convers. Manage.*, **48**, 1525 (2007).
28. T. W. Song, J. L. Sohn, J. H. Kim, T. S. Kim, S. T. Ro and K. Suzuki, *J. Power Sources*, **142**(1-2), 30 (2005).
29. P. Costamagna, L. Magistri and A. F. Massardo. *J. Power Sources*, **96**(2), 352 (2001).
30. L. Petruzzi, S. Cocchi and F. Fineschi, *J. Power Sources*, **118**(1-2), 96 (2003).
31. M. Pfafferodt, P. Heidebrecht, M. Stelter and K. Sundmacher, *J. Power Sources*, **149**, 53 (2005).
32. A. Ringuede, D. Bronine and J. R. Frade, *Solid State Ionics*, **146**(3-4), 219 (2002).